Available online at www.sciencedirect.com
ScienceDirect
Comput. Methods Appl. Mech. Engrg. 197 (2008) 567–576
Computer methods in applied mechanics and engineering
www.elsevier.com/locate/cma

Some improvements to the flux-type a posteriori error estimators

Xiaoliang Wan

Division of Applied Mathematics, Brown University, Providence, RI 02912, USA

Received 2 February 2007; received in revised form 19 July 2007; accepted 14 August 2007
Available online 12 September 2007

Abstract

This paper presents explicit equilibrated fluxes for the local pure-Neumann problems used by the a posteriori error estimator in Ainsworth and Oden [M. Ainsworth, J.T. Oden, A procedure for a posteriori error estimation for *h–p* finite element methods, Comput. Methods Appl. Mech. Engrg. 101 (1992) 73–96]. We modify the target function for minimization to obtain new equilibrated fluxes in a weighted form. We investigate the performance of the new equilibrated fluxes in two-dimensional spectral/*hp* element approximations of an elliptic equation using conforming triangle elements. The new fluxes appear more robust and lead to substantial computational savings compared to the original numerical procedure in Ainsworth and Oden [Ainsworth and Oden et al., 1992].

Keywords: Finite elements; Spectral elements; Elliptic equations

1. Introduction

A posteriori error estimation has become an important tool in the finite element method, as it can be used to control the numerical errors and guide goal-oriented mesh adaptivity strategies. Many a posteriori error estimators have been developed (see [2–4] and references therein), which are mainly based on the residual method [5–9] or on the recovery method [10,11]. Recently, a new approach referred to as goal-oriented error estimation has been developed, which measures the error of a linear functional of the solution rather than the usual energy norm (see [3,12,13] and references therein).

Among the residual type a posteriori error estimators the equilibrated method [6,7] is now accepted as the most effective one, as it can be applied reliably to *hp* finite element methods. The equilibrated residual method is based on the solutions of local Neumann type boundary-value problems, where the proper flux boundary conditions are usually obtained by post-processing the finite element approximation. Such an idea goes back to the work in [14,15,8]. In this paper we investigate the performance of the equilibrated residual method proposed in [6,7] for the spectral/*hp* element method [16]. To obtain consistent flux conditions a singular linear system needs to be solved. In [7], a numerical procedure was proposed. To avoid solving such a singular linear system numerically, we derive the equilibrated fluxes in an explicit form for the two-dimensional finite elements. We subsequently introduce some weights [17] into the target function for minimization and obtain new equilibrated fluxes in a weighted form. We compare the performance of the new fluxes with that given in [6] using elliptic problems with smooth and singular solutions. It appears that the new fluxes are less sensitive to the deformation of the finite elements with low-order polynomials; for *p*-version finite elements it is not so important how to determine the equilibration because the approximation solution can provide a good approximation of flux. Furthermore, the cost for the equilibrated fluxes is reduced to $O(N_{\text{patch}})$ for each interior vertex, where N_{patch} is the number of elements forming the support of the corresponding linear shape function.

This paper is organized as follows: in the next section we present the model problem and provide the polynomial space used in this work. In Section 3, we derive explicit

E-mail address: xlwan@dam.brown.edu

0045-7825/$ - see front matter © 2007 Elsevier B.V. All rights reserved.
doi:10.1016/j.cma.2007.08.015

equilibrated fluxes for the procedure given in [6] and propose a weighted target function to determine the flux equilibration. We study the new a posteriori error estimator numerically in Section 5. We summarize and conclude our work in Section 6.

2. Model problem and its discretization

Let $\Omega \subset \mathbb{R}^2$ be a bounded domain with a Lipschitz boundary $\partial\Omega$. We consider the following elliptic boundary-value problem:

$$-\Delta u + cu = f \quad \text{in } \Omega, \tag{1a}$$

$$\frac{\partial u}{\partial \boldsymbol{n}} = g \quad \text{on } \Gamma_N, \tag{1b}$$

$$u = 0 \quad \text{on } \Gamma_D, \tag{1c}$$

where the boundary segments Γ_N and Γ_D are disjoint with $\overline{\Gamma}_N \cup \overline{\Gamma}_D = \partial\Omega$ and c is a nonnegative constant. We assume that $f \in L_2(\Omega)$ and $g \in L_2(\Gamma_N)$ guarantee a unique solution u. Let

$$V = \{v \in H^1(\Omega) : v|_{\Gamma_D} = 0\}.$$

The weak form for the model problem (1a) is to find $u \in V$ such that

$$\mathscr{B}(u, v) = \mathscr{L}(v) \quad \forall v \in V, \tag{2}$$

where

$$\mathscr{B}(u, v) = \int_\Omega (\nabla u \cdot \nabla v + cuv)\mathrm{d}\boldsymbol{x} \tag{3}$$

and

$$\mathscr{L}(v) = \int_\Omega fv\,\mathrm{d}\boldsymbol{x} + \int_{\Gamma_N} gv\,\mathrm{d}s. \tag{4}$$

Let $\mathscr{T}_h$ be a family of triangulations of Ω with straight edges. We assume that the family is regular, in other words, the minimal angle of all the triangles is bounded from below by a positive constant. However, the meshes are not assumed to be quasiuniform. We define the finite element space as

$$V_h^K = \{v : v \circ F_K^{-1} \in \mathscr{P}_p(R)\},$$

$$V_h = \{v \in H^1(\Omega) : v|_K \in V_h^K, K \in \mathscr{T}_h\},$$

where F_K is the mapping function for the element K which maps the the reference element R to element K and $\mathscr{P}_p(R)$ denotes the set of polynomials of degree up to p over R. We assume that $v_h|_{\Gamma_D} = 0, \forall v_h \in V_h$. The finite element solution u_h satisfies:

Find $u_h \in V_h$ such that

$$\mathscr{B}(u_h, v_h) = \mathscr{L}(v_h), \quad \forall v_h \in V_h. \tag{5}$$

2.1. Reference elements

In this work we employ the spectral/*hp* element spaces defined in [16] for $\mathscr{P}_p(R)$.

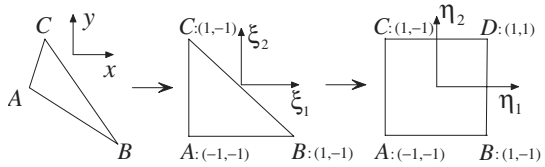

Fig. 1. Mapping between triangular elements and the reference element.

For a triangular reference domain, see Fig. 1, a hierarchical set of basis is given as

$$\text{Vertex A}: \frac{1-\eta_1}{2}\frac{1-\eta_2}{2},$$

$$\text{Vertex B}: \frac{1+\eta_1}{2}\frac{1-\eta_2}{2},$$

$$\text{Vertex C}: \frac{1+\eta_2}{2},$$

$$\text{Edge AB}: \frac{1-\eta_1}{2}\frac{1+\eta_1}{2}P_{p-1}^{1,1}(\eta_1)\left(\frac{1-\eta_2}{2}\right)^{p+1} \quad (0 < p < P_1),$$

$$\text{Edge AC}: \frac{1-\eta_1}{2}\frac{1-\eta_2}{2}\frac{1+\eta_2}{2}P_{q-1}^{1,1}(\eta_2) \quad (0 < q < P_2),$$

$$\text{Edge BC}: \frac{1+\eta_1}{2}\frac{1-\eta_2}{2}\frac{1+\eta_2}{2}P_{q-1}^{1,1}(\eta_2) \quad (0 < q < P_2),$$

$$\text{Interior}: \frac{1-\eta_1}{2}\frac{1+\eta_1}{2}P_{p-1}^{1,1}(\eta_1)\left(\frac{1-\eta_2}{2}\right)^{p+1}\frac{1+\eta_2}{2}P_{q-1}^{2p+1,1}(\eta_2),$$

$$(0 < p, q; p < P_1; p + q < P_2, P_1 \leqslant P_2)$$

subject to the mapping

$$\eta_1 = 2\frac{1+\xi_1}{1-\xi_2} - 1, \quad \eta_2 = \xi_2,$$

where $P_p^{\alpha,\beta}$ denotes pth order one-dimensional Jacobi polynomials on $(-1, 1)$ with indexes α and β.

3. An element-residual a posteriori error estimator

Let $e = u - u_h$ denote the error for the finite element solution u_h. The error e satisfies the following boundary value problem in element K

$$\mathscr{B}_K(e, v) = (f, v)_K - \mathscr{B}_K(u_h, v) + \int_{\partial K} v(\boldsymbol{n}_K \cdot \nabla u)\mathrm{d}s, \quad \forall v \in V(K), \tag{6}$$

where

$$V(K) = \{v : v = w|_K, \forall w \in V\}$$

$$\mathscr{B}_K(u, v) = \int_K (\nabla u \cdot \nabla v + cuv)\mathrm{d}\boldsymbol{x}$$

$$(f, v)_K = \int_K fv\,\mathrm{d}\boldsymbol{x}.$$

We note here that the flux on ∂K (last term in Eq. (6)) is, in general, unknown and needs to be constructed. By replacing the true Neumann boundary data with an approxima-

tion $g_K \approx \boldsymbol{n}_K \cdot \nabla u|_K$, we obtain a local pure-Neumann boundary value problem

$$\mathscr{B}_K(\phi_K, v) = (f, v)_K - \mathscr{B}_K(u_h, v) + \int_{\partial K} v g_K \, \mathrm{d}s, \quad \forall v \in V(K). \tag{7}$$

The solution ϕ_K is an approximation to the true error on the element K. It is known that if $c = 0$, the equilibration condition

$$(f, 1)_K - \mathscr{B}_K(u_h, 1) + \int_{\partial K} g_K \, \mathrm{d}s = 0, \tag{8}$$

must be satisfied by g_K for the existence of a solution ϕ_K. In [3], a stronger condition

$$(f, v)_K - \mathscr{B}_K(u_h, v) + \int_{\partial K} g_K v \, \mathrm{d}s = 0, \quad \forall v \in V_h^K \tag{9}$$

was used to deal with general *hp* finite elements, which is obviously a sufficient condition of Eq. (8). Also, g_K should satisfy the consistency condition

$$\sum_{K \in \mathscr{T}_h} \int_{\partial K} g_K v \, \mathrm{d}s = \int_{\Gamma_N} g v \, \mathrm{d}s, \quad \forall v \in V. \tag{10}$$

Once the equilibrated fluxes g_K are determined, we can obtain a unique solution ϕ_K of the local problem (7). Let $|||\cdot|||$ denote the global energy norm and $|||\cdot|||_K$ the local one. Based on $\{\phi_K\}$, the upper bound of $|||e|||$ can be guaranteed by the following theorem.

Theorem 1 (cf. [3]). *Suppose that g_K are a set of equilibrated fluxes. The global error residual can be decomposed into local contributions*

$$\mathscr{B}(e, v) = \sum_{K \in \mathscr{T}_h} \mathscr{B}_K(\phi_K, v), \quad v \in V,$$

where $\phi_K \in V(K)$ is the solution of the local problem (7). The global error in the finite element approximation may be bounded by

$$|||e|||^2 \leqslant \sum_{K \in \mathscr{T}_h} |||\phi_K|||_K^2. \tag{11}$$

3.1. Revisiting the Ainsworth–Oden (A–O) procedure for flux splitting

For any $K \in \mathscr{T}_h$ we denote by $\mathscr{E}(K)$ and $\mathscr{N}(K)$ the sets of its edges and vertices, respectively. Let $\mathscr{E}_h = \cup_{K \in \mathscr{T}_h} \mathscr{E}(K)$ and $\mathscr{N}_h = \cup_{K \in \mathscr{T}_h} \mathscr{N}(K)$. We assume that all vertices in $\mathscr{N}_h$ are regular nodes without hanging nodes. For each $\boldsymbol{x}_n \in \mathscr{N}_h$ we define an *element patch* $\mathscr{P}_n$ as

$$\mathscr{P}_n = \{K : \boldsymbol{x}_n \in \mathscr{N}(K), \forall K \in \mathscr{T}_h\}$$

and an *edge patch* $\mathscr{E}_n$ as

$$\mathscr{E}_n = \{\gamma : \boldsymbol{x}_n \in \mathscr{N}(E), \forall E \in \mathscr{E}_h\}.$$

Let $\mathscr{E}_n = \mathscr{E}_n^I \cup \mathscr{E}_n^N \cup \mathscr{E}_n^D$, where

$$\mathscr{E}_n^N = \{\gamma \in \mathscr{E}_n : \gamma \subset \partial K \cap \Gamma_N, K \in \mathscr{P}_n\}$$
$$\mathscr{E}_n^D = \{\gamma \in \mathscr{E}_n : \gamma \subset \partial K \cap \Gamma_D, K \in \mathscr{P}_n\}$$

and $\mathscr{E}_n^I = \mathscr{E}_n \setminus \mathscr{E}_n^N \setminus \mathscr{E}_n^D$. We note here that there exists one-to-one correspondence between $\boldsymbol{x}_n$ and $\mathscr{P}_n$.

We here focus on the fluxes for the linear shape functions $\{\theta_n\}$ corresponding to interior vertices. In Fig. 2, a patch associated with an interior vertex is shown.

Let $\mu_{K,n}^{\gamma} = \int_{\gamma} g \theta_n \, \mathrm{d}s$ denote the flux moment on edge γ. Then the equilibration condition (9) and consistency condition (10) are equivalent to the following two lemmas [7,3], respectively.

Lemma 2. *Let $\{\theta_n : n \in \mathscr{N}(K)\}$ be a basis for the local finite element space V_h^K on element K. The equilibration condition (9) holds on K if and only if*

$$\sum_{\gamma \subset \partial K} \mu_{K,n}^{\gamma} = \Delta_K(\theta_n) \quad \forall n \in \mathscr{N}(K), \tag{12}$$

with $\Delta_K(v)$ being the element residual

$$\Delta_K(v) = \mathscr{B}_K(u_h, v) - (f, v)_K. \tag{13}$$

Lemma 3. *The consistency condition (10) holds if and only if the fluxes g_K satisfy*

$$g_K = g \quad \text{on } \partial K \cap \Gamma_N$$
$$g_K + g_{K'} = 0 \quad \text{on } \partial K \cap \partial K',$$

which yields that

$$\mu_{K,n}^{\gamma} = \int_{\gamma} g \theta_n \, \mathrm{d}s, \quad \gamma = \partial K \cap \Gamma_N$$
$$\mu_{K,n}^{\gamma} + \mu_{K',n}^{\gamma} = 0, \quad \gamma = \partial K \cap \partial K'.$$

Let $\tilde{\mu}_{K,n}^{\gamma} = \int_{\gamma} \theta_n (\boldsymbol{n}_K \cdot \nabla u_h|_K) \mathrm{d}s$ denote the approximate flux moments. $\mu_{K,n}^{\gamma}$ related to the vertex modes are selected by the following problem [3]:

$$\left.\begin{array}{ll} \text{Minimize} & \frac{1}{2} \sum\limits_{K \in \mathscr{P}_n} \sum\limits_{\gamma \in \mathscr{E}_n \cap \partial K} (\mu_{K,n}^{\gamma} - \tilde{\mu}_{K,n}^{\gamma})^2 \\ \text{subject to} & \sum\limits_{\gamma \in \mathscr{E} \cap \partial K} \mu_{K,n}^{\gamma} = \Delta_K(\theta_n) \quad \text{for all } K \in \mathscr{P}_n \\ \text{with} & \mu_{K,n}^{\gamma} = \int_{\gamma} g \theta_n \, \mathrm{d}s \quad \text{on } \gamma \in \mathscr{E}_n^N \cap \partial K \\ \text{and} & \mu_{K,n}^{\gamma} + \mu_{K',n}^{\gamma} = 0 \quad \text{on } \gamma \in \mathscr{E}_n^I \cap \partial K \cap \partial K' \end{array}\right\} \tag{14}$$

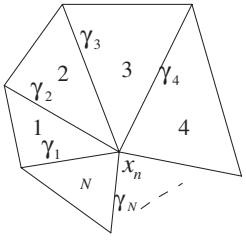

Fig. 2. The patches $\mathscr{P}_n$ and $\mathscr{E}_n$ of elements and edges influenced by the basis function θ_n associated with an interior vertex located at $\boldsymbol{x}_n$.

The problem (14) leads to the following conditions satisfied by the Lagrange multipliers $\{\sigma_{K,n} : K \in \mathscr{P}_n\}$ (see [3] for more details):

$$\sum_{K':\partial K\cap\partial K'\in\mathscr{E}_n^I}(\sigma_{K,n}-\sigma_{K',n})+2\sum_{\gamma:\gamma\cap\partial K\in\mathscr{E}_n^D}\sigma_{K,n}=\tilde{\Delta}_K(\theta_n),\quad \forall K\in\mathscr{P}_n, \tag{15}$$

where $\tilde{\Delta}_K(\theta_n)$ are modified element residuals

$$\tilde{\Delta}_K(\theta_n)=2\left[\mathscr{B}_K(u_h,\theta_n)-(f,\theta_n)_K-\int_{\partial K}\left\langle\frac{\partial u_X}{\partial \boldsymbol{n}_K}\right\rangle\theta_n\,\mathrm{d}s\right]$$

and the average flux is defined as

$$\left\langle\frac{\partial u_X}{\partial \boldsymbol{n}_K}\right\rangle=\begin{cases}\frac{1}{2}\left(\frac{\partial u_n}{\partial \boldsymbol{n}_K}|_K+\frac{\partial u_n}{\partial \boldsymbol{n}_K}|_{K'}\right) & \gamma\in\mathscr{E}_n^I\cap\partial K\cap\partial K'\\ g & \gamma\in\mathscr{E}_n^N\cap\partial K\\ \frac{\partial u_h}{\partial \boldsymbol{n}_K} & \gamma\in\mathscr{E}_n^D\cap\partial K.\end{cases}$$

Then the equilibrated fluxes can be expressed as

$$\mu_{K,n}^{\gamma}=\begin{cases}\frac{1}{2}(\sigma_{K,n}-\sigma_{K',n})+\frac{1}{2}(\tilde{\mu}_{K,n}^{\gamma}-\tilde{\mu}_{K',n}^{\gamma}) & \gamma\in\mathscr{E}_n^I\cap\partial K\cap\partial K'\\ \int_\gamma g\theta_n\,\mathrm{d}s & \gamma\in\mathscr{E}_n^N\cap\partial K\\ \sigma_{K,n}+\tilde{\mu}_{K,n}^{\gamma} & \gamma\in\mathscr{E}_n^D\cap\partial K.\end{cases} \tag{16}$$

3.2. Explicit equilibrated fluxes

We denote the linear system (15) in matrix form as

$$\boldsymbol{T}_n\boldsymbol{\sigma}_n=\tilde{\boldsymbol{\Delta}}_n, \tag{17}$$

For an interior vertex shown in Fig. 2, $\boldsymbol{T}_n$ takes the form

$$\boldsymbol{T}_n=\begin{bmatrix}2&-1&&\cdots&&-1\\-1&2&-1&\cdots&&0\\\vdots&&&&&\vdots\\0&&\cdots&-1&2&-1\\-1&&\cdots&&-1&2\end{bmatrix},$$

where $\boldsymbol{T}_n$ is singular with a one-dimensional kernel $\dim(\ker(\boldsymbol{T}_n))=1$. We note that T is a circulant matrix corresponding to a finite difference scheme subject to periodic boundary conditions. The eigenvalues and eigenvectors of such a matrix can be found in [18]. We are interested in the explicit formulas of $(\sigma_{n,i}-\sigma_{n,i+1})$. It is easy to verify that the solvability condition $\sum_{K\in\mathscr{P}_n}\tilde{\Delta}_K=0$ is satisfied due to the Galerkin projection. In [7] a procedure was proposed to pick up a solution in a least-squares sense. However, such a procedure would give rise to more cost compared to classical element residual estimators. Here we present the equilibrated fluxes in an explicit form for the two-dimensional case.

Lemma 4. *For the patch shown in Fig. 2, the following relations satisfy Eq. (17)*

$$\sigma_{n,i}-\sigma_{n,i+1}=\frac{\tilde{\Delta}_{n,i}-\sum_{j=2}^{N-1}(N-j)\tilde{\Delta}_{n,\overline{\mathrm{mod}}(j+i-1,N)}}{N}, \tag{18}$$

where $i=1,2,\ldots,N-1$ *and*

$$\overline{\mathrm{mod}}(m,N)=\begin{cases}\mathrm{mod}(m+kN,N) & \text{if } \mathrm{mod}(m+kN,N)\neq 0;\\ N & \text{otherwise,}\end{cases}$$

with k *being any integer to make* $m+kN>0$. *Furthermore, the relations (18) are uniquely determined by Eq. (17). From now on, we replace the symbol* K_i *with* i *in the subscripts of* $\sigma_{K_i,n}$ *and* $\tilde{\Delta}_{K_i,n}$ *for convenience.*

Proof. We first verify that the relations (18) satisfy the system (17). It is easy to obtain that

$$\begin{aligned}&-(\sigma_{n,i}-\sigma_{n,i+1})+(\sigma_{n,i+1}-\sigma_{n,i+2})\\&=\frac{-\tilde{\Delta}_{n,i}+\sum_{j=2}^{N-1}(N-j)\tilde{\Delta}_{n,\overline{\mathrm{mod}}(j+i-1,N)}}{N}\\&\quad+\frac{\tilde{\Delta}_{n,i+1}-\sum_{j=2}^{N-1}(N-j)\tilde{\Delta}_{n,\overline{\mathrm{mod}}(j+i,N)}}{N}\\&=\frac{N\tilde{\Delta}_{n,i+1}-\sum_{j=1}^{N}\tilde{\Delta}_{n,i}}{N}=\tilde{\Delta}_{n,i+1}.\end{aligned}$$

Due to symmetry, we know that all equations in system (17) are satisfied. We next show that the relations (18) are uniquely determined by the system (17). Let

$$\hat{\boldsymbol{\sigma}}_n=\boldsymbol{A}\boldsymbol{\sigma}_n,$$

where

$$\boldsymbol{A}=\begin{bmatrix}1&-1&0&\cdots&&0\\0&1&-1&\cdots&&0\\\vdots&&&&&\vdots\\0&&\cdots&&1&-1\\0&&\cdots&&0&1\end{bmatrix},\quad \hat{\boldsymbol{\sigma}}_n=\begin{bmatrix}\sigma_{n,1}-\sigma_{n,2}\\\sigma_{n,2}-\sigma_{n,3}\\\vdots\\\sigma_{N-1}-\sigma_N\\\sigma_N\end{bmatrix}.$$

It is easy to obtain the inverse of $\boldsymbol{A}$ as

$$\boldsymbol{A}^{-1}=\begin{bmatrix}1&1&1&\cdots&&1\\0&1&1&\cdots&&1\\\vdots&&&&&\vdots\\0&&\cdots&&1&1\\0&&\cdots&&0&1\end{bmatrix}.$$

Thus, the system (17) can be rewritten as

$$\begin{bmatrix}2&1&1&\cdots&1&0\\-1&1&0&\cdots&0&0\\\vdots&&&&&\vdots\\0&&\cdots&-1&1&0\\-1&-1&\cdots&&-2&0\end{bmatrix}\begin{bmatrix}\sigma_1-\sigma_2\\\sigma_2-\sigma_3\\\vdots\\\sigma_{N-1}-\sigma_N\\\sigma_N\end{bmatrix}=\begin{bmatrix}\tilde{\Delta}_{n,1}\\\tilde{\Delta}_{n,2}\\\vdots\\\tilde{\Delta}_{n,N-1}\\\tilde{\Delta}_{n,N}\end{bmatrix}.$$

Since $\dim(\ker(\boldsymbol{T}_n)) = 1$, we only need to consider the first $N-1$ equations, which yield a linear system related to $\sigma_{n,i} - \sigma_{n,i+1}$

$$\boldsymbol{B}\hat{\boldsymbol{\sigma}}_n = \begin{bmatrix} 2 & 1 & 1 & \cdots & 1 \\ -1 & 1 & 0 & \cdots & 0 \\ \vdots & & & & \vdots \\ 0 & 0 & \cdots & -1 & 1 \end{bmatrix} \begin{bmatrix} \sigma_1 - \sigma_2 \\ \sigma_2 - \sigma_3 \\ \vdots \\ \sigma_{N-1} - \sigma_N \end{bmatrix} = \begin{bmatrix} \tilde{\Delta}_{n,1} \\ \tilde{\Delta}_{n,2} \\ \vdots \\ \tilde{\Delta}_{n,N-1} \end{bmatrix}.$$

Since $\det(\boldsymbol{B}) = N$, the conclusion follows immediately.

To this end, we have obtained the explicit forms of equilibrated fluxes for the interior vertex.

3.2.1. Two-dimensional flux splitting based on weighted target functions

In [6] the non-uniqueness of equilibrated fluxes is removed by minimizing the value of

$$\frac{1}{2}\sum_{K\in\mathscr{P}_n}\sum_{\gamma\in\mathscr{E}_n\cap\partial K}(\mu^{\gamma}_{K,n} - \tilde{\mu}^{\gamma}_{K,n})^2. \tag{19}$$

By noting that the function θ_n introduces a factor $l(\gamma)$ (length of γ) into $\mu^{\gamma}_{K,n}$, we use a weighted version of Eq. (19) as

$$\frac{1}{2}\sum_{K\in\mathscr{P}_n}\sum_{\gamma\in\mathscr{E}_n\cap\partial K} w_i^2(\mu^{\gamma}_{K,n} - \tilde{\mu}^{\gamma}_{K,n})^2, \tag{20}$$

where we add weights w_i into Eq. (19). In this work we investigate a weight factor $w_i = \frac{1}{l(\gamma)}$ with $\gamma \in \mathscr{E}_n \cap \partial K_i$. By noting that $\int_\gamma \theta_n \,\mathrm{d}s = \frac{l(\gamma)}{2}$, it is clear that we are minimizing the difference between the mean values of true fluxes $\frac{\partial u}{\partial \boldsymbol{n}_K}$ and numerical fluxes $\frac{\partial u_h}{\partial \boldsymbol{n}_K}$ with respect to θ_n along the edges $\gamma \in \mathscr{E}_n$. It was shown in [19] that such a weight factor can improve the performance of the residual-type a posteriori error estimator proposed in [14]. We subsequently present the explicit equilibrated fluxes corresponding to the weighted target function (20) and investigate the influence of the weights on the performance of a posteriori error estimator given by Theorem 1.

Following a similar procedure as in [3], we can derive the equilibrated fluxes as

$$\mu^{\gamma}_{K,n} = \begin{cases} \frac{1}{2}l_\gamma^2(\sigma_{K,n} - \sigma_{K',n}) + \frac{1}{2}(\tilde{\mu}^{\gamma}_{K,n} - \tilde{\mu}^{\gamma}_{K',n}) & \gamma \in \mathscr{E}_n^I \cap \partial K \cap \partial K' \\ \int_\gamma g\theta_n \,\mathrm{d}s & \gamma \in \mathscr{E}_n^N \cap \partial K \\ l_\gamma^2\sigma_{K,n} + \tilde{\mu}^{\gamma}_{K,n} & \gamma \in \mathscr{E}_n^D \cap \partial K \end{cases}. \tag{21}$$

where $\sigma_{K,n}$ must satisfy

$$\frac{1}{2}\sum_{\gamma:\gamma\cap\partial K\cap\partial K'\in\mathscr{E}_n^I} l_\gamma^2(\sigma_{K,n} - \sigma_{K',n}) + \sum_{\gamma:\gamma\cap\partial K\in\mathscr{E}_n^D} l_\gamma^2\sigma_{n,i} = \tilde{\Delta}_K(\theta_n). \tag{22}$$

For the patch $\mathscr{P}_n$ corresponding to an interior vertex, $\boldsymbol{T}_n$ in Eq. (17) takes the form

$$\boldsymbol{T}_n = \begin{bmatrix} l_{\gamma_1}^2 + l_{\gamma_2}^2 & -l_{\gamma_1}^2 & & \cdots & & -l_{\gamma_1}^2 \\ -l_{\gamma_2}^2 & l_{\gamma_2}^2 + l_{\gamma_3}^2 & -l_{\gamma_3}^2 & \cdots & & 0 \\ \vdots & & & & & \vdots \\ 0 & & \cdots & -l_{\gamma_{N-1}}^2 & l_{\gamma_{N-1}}^2 + l_{\gamma_N}^2 & -l_{\gamma_N}^2 \\ -l_{\gamma_1}^2 & & \cdots & & -l_{\gamma_N}^2 & l_{\gamma_N}^2 + l_{\gamma_1}^2 \end{bmatrix}.$$

Using the similar idea as in the proof of Lemma 4, it can be proved that:

Lemma 5. *For the patch shown in Fig. 2, the following relations are uniquely determined by Eq. (22)*

$$\sigma_{n,i} - \sigma_{n,i+1} = \frac{\tilde{\Delta}_{n,i} - \sum_{j=2}^{N-1}\tilde{\Delta}_{n,\overline{\mathrm{mod}}(j+i-1,N)}H_{i,j}}{l_{\gamma_1}^2 l_{\gamma_2}^2 \sum_{i=1}^{N}\frac{1}{l_{\gamma_i}^2}}, \tag{23}$$

where

$$H_{i,j} = \sum_{k=1}^{N-j}\frac{l_{\gamma_i}^2}{l_{\gamma_{\overline{\mathrm{mod}}(i-k,N)}}^2}. \tag{24}$$

3.2.2. High-order equilibration conditions

We now consider the equilibration condition for the edge modes. Due to the Galerkin projection, the high-order equilibration actually looks trivial, see [1,3]. We here summarize the results as

Lemma 6. *Given an element K and edge modes θ_n, the equilibrated flux moments can be expressed as*

$$\begin{aligned} \mu^{\gamma}_{K,n} &= \Delta_K \quad \gamma \in \partial K \cap (\mathscr{E}_n^I \cup \mathscr{E}_n^D), \\ \mu^{\gamma}_{K,n} &= \int_\gamma g\theta_n \,\mathrm{d}s \quad \gamma \in \partial K \cap \mathscr{E}_n^N, \end{aligned} \tag{25}$$

where

$$\Delta_K(\theta_n) = \mathscr{B}_K(u_h, \theta_n) - (f, \theta_n)_K. \tag{26}$$

Remark 7. Explicit fluxes for elements with hanging nodes. In the adaptive mesh refinement, it is convenient to use meshes with hanging nodes. We expect to obtain the explicit forms of equilibrated fluxes for such kinds of finite element meshes. Actually it can be done easily using the idea of macro-element defined in [3], if we assume that there exists at most one hanging node on an edge. The macro-element is defined as follows (see Fig. 3 for an example [3]): "If $\boldsymbol{x}_n$ is a hanging node, the macro-element $K_n^* = K$ with K being an element containing the node $\boldsymbol{x}_n$; otherwise, K_n^* is the domain formed from K and elements having a hanging node in common with K, but not containing the node $\boldsymbol{x}_n$ itself."

We note that there are no hanging nodes any more on the edges of macro-elements. The point is that if we define the element patch $\mathscr{P}_n$ and $\mathscr{E}_n$ using the macro-elements we can get the explicit equilibrated fluxes on edges of the

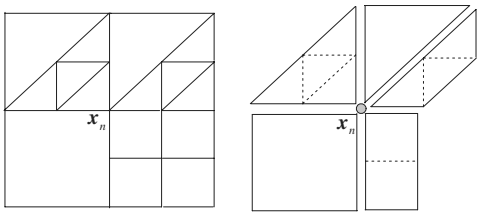

Fig. 3. Left: a mesh with hanging nodes. Right: the patch $\mathscr{P}_n$ consisting of macro-elements associated with vertex x_n.

macro-elements for θ_n using the formulas in Lemmas 4 and 5. Subsequently, we can follow the procedure given in [3] (see Section 6.6.4) to recover explicitly the equilibrated fluxes for edges with hanging nodes.

3.2.3. Computational cost

We consider here only the cost for the first-order equilibrated fluxes, which is the dominant part for the flux equilibration. We assume that the usual type of small angle condition is satisfied and the number of elements forming the support of any linear shape function θ_n is bounded above by N_{patch} independently of the mesh size. To obtain $(\sigma_{n,i} - \sigma_{n,i+1})$ a cost of order N_{patch} is needed (see Lemma 4). Using the relation $\sigma_{n,i+1} - \sigma_{n,i+2} = \tilde{\Delta}_{n,i+1} + (\sigma_{n,i} - \sigma_{n,i+1})$ recursively, we can obtain the equilibrated fluxes moments $\mu^{\gamma}_{n,i}$ for each patch by a total cost of $O(2N_{\text{patch}})$ compared to the cost of $O(\frac{1}{3}N^3_{\text{patch}} + \frac{1}{2}N^2_{\text{patch}})$ given in [7], where $\sigma_{n,i}$ is computed numerically. Thus, the cost can be reduced significantly by using the explicit solutions of equilibrated flux moments.

4. Non-homogeneous Dirichlet boundary conditions

In last section we assume that the Dirichlet boundary conditions are homogeneous. However, the Dirichlet boundary conditions are, in general, non-homogeneous, which implies that the approximation error of Dirichlet boundary conditions should be taken into account for the a posteriori error estimate. In fact, such an error can affect the effectiveness of a posteriori error estimators significantly in some cases, e.g., linear finite elements. In this work, we use the method given in [20] to decompose the error e into two parts as

$$e = e_G + e_D,$$

where the *Galerkin error*, $e_G \in H^1_0(\Omega)$, satisfies

$$\mathscr{B}(e_G, v) = \mathscr{B}(e, v) \quad \forall v \in H^1_0(\Omega) \tag{27}$$

and the *Dirichlet error*, $e_D \in H^1(\Omega)$, satisfies

$$\begin{aligned} &\mathscr{B}(e_D, v) = \mathscr{B}(e, v) - \mathscr{B}(e_G, v) = 0 \quad \forall v \in H^1_0(\Omega) \\ &e_D = q - q_h \quad \text{on } \Gamma_D, \end{aligned} \tag{28}$$

where q and q_h are the true and approximated Dirichlet boundary conditions. Following these definitions, it can be shown [20] that in the energy norm

$$|||e|||^2 = |||e_G|||^2 + |||e_D|||^2. \tag{29}$$

$|||e_G|||$ can be bounded using the equilibrated residual method described in last section; $|||e_D|||$ can be readily bounded by

$$|||e_D|||^2 \leqslant \sum_{K \in \mathscr{T}_h} |||\psi_K|||^2, \tag{30}$$

where ψ_K is the solution of the local problems

$$\begin{aligned} &\mathscr{B}_K(\psi_K, v) = 0 \quad \forall v \in H^1_0(K) \\ &\psi_K = \begin{cases} e_D & \text{on } \partial K \cap \Gamma_D \\ 0 & \text{on } \partial K \setminus \Gamma_D. \end{cases} \end{aligned} \tag{31}$$

Since such local problems are solved only in the Dirichlet boundary elements, the cost for e_D is usually much smaller than that for e_G.

5. Numerical examples

In this section we demonstrate numerically the influence of weights we put into the A–O procedure.

5.1. Efficiency for smooth solutions

We first consider a symmetric elliptic operator with a smooth solution [1]:

$$-\Delta u + u = 0 \quad \text{in } \Omega \tag{32}$$

subject to the boundary conditions

$$\begin{aligned} &u(0, y) = \left(e^{-\sqrt{1+4\pi^2}} + 1\right) \sin 2\pi y, \quad 0 < y < 1/2, \\ &u(x, 0) = u(0, 1/2) = 0, \quad 0 < x < 1/2, \\ &\partial u / \partial \boldsymbol{n} = 0, \quad x = 1/2, \quad 0 < y < 1/2. \end{aligned} \tag{33}$$

The true solution for this problem is

$$\begin{aligned} u(x, y) = &\left(\exp\left((x-1)\sqrt{1+4\pi^2}\right)\right. \\ &\left. + \exp\left(-x\sqrt{1+4\pi^2}\right)\right) \sin 2\pi y. \end{aligned} \tag{34}$$

We study this problem numerically using the periodic cell patterns [19] in Fig. 4, which consist of triangle elements. The computation domain Ω is decomposed by one of these cells periodically. We control the deformation of triangle elements by the ratio a/b. In this work we basically check two cases: $a/b = 1$ and $a/b = 4$. We denote the decomposition of the computation domain Ω by a cell matrix (M,N), where M is the number of cells in the y-direction and N is the number of cells in the x-direction. Thus, the total elements number is $N_c MN$, where N_c is the number of elements in a certain cell pattern. Let $|||e_h|||/|||e|||$ be the effectivity index, which is the ratio of estimated error over the true error. We use $E_{k,s}$ to denote the effectivity index from the weighted fluxes and $E_{o,s}$ from the A–O procedure, where s indicates the cell patterns from (a) to (f).

For linear elements we enrich the local finite element space $V^K_h(v)$ by polynomial order 1 or 2. In Tables 1–4,

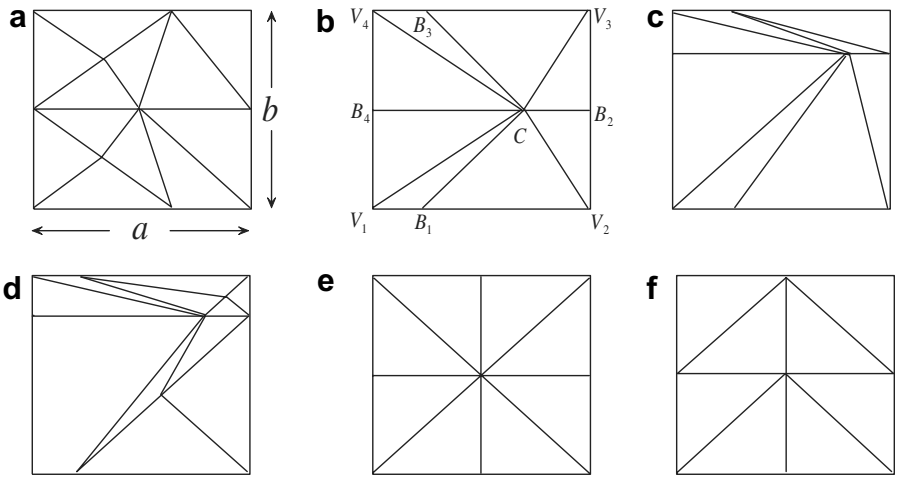

Fig. 4. Different cell patterns consisting of triangle elements.

Table 1
Effectivity indices for cell pattern (a)–(c)

(M,N)	$E_{k,a}$	$E_{o,a}$	$E_{k,b}$	$E_{o,b}$	$E_{k,c}$	$E_{o,c}$
(1,1)	1.088	1.086	0.999	1.015	1.414	1.232
(2,2)	1.045	1.045	1.074	1.049	1.135	1.107
(3,3)	1.029	1.030	1.077	1.045	1.111	1.120
(4,4)	1.021	1.023	1.077	1.044	1.103	1.130
(4,1)	0.954	0.908	1.191	1.324	1.129	1.145
(8,2)	0.946	0.925	1.102	1.287	1.083	1.145
(12,3)	0.946	0.933	1.092	1.274	1.092	1.155
(16,4)	0.946	0.939	1.096	1.259	1.113	1.165

Linear elements and increment of polynomial order 1 are considered.

Table 2
Effectivity indices for cell pattern (d)–(f)

(M,N)	$E_{k,d}$	$E_{o,d}$	$E_{k,e}$	$E_{o,e}$	$E_{k,f}$	$E_{o,f}$
(1,1)	1.931	1.859	1.009	1.010	1.048	1.045
(2,2)	1.309	1.603	1.031	1.031	1.030	1.029
(3,3)	1.233	1.514	1.024	1.024	1.021	1.021
(4,4)	1.196	1.452	1.020	1.020	1.017	1.018
(4,1)	0.965	2.081	1.214	1.379	1.148	1.032
(8,2)	1.016	1.812	1.275	1.495	1.089	1.012
(12,3)	1.028	1.679	1.327	1.537	1.068	1.008
(16,4)	1.030	1.586	1.362	1.555	1.057	1.007

Linear elements and increment of polynomial order 1 are considered.

Table 3
Effectivity indices for cell pattern (a)–(c)

(M,N)	$E_{k,a}$	$E_{o,a}$	$E_{k,b}$	$E_{o,b}$	$E_{k,c}$	$E_{o,c}$
(1,1)	1.192	1.191	1.057	1.056	1.553	1.294
(2,2)	1.163	1.163	1.176	1.160	1.339	1.252
(3,3)	1.148	1.149	1.201	1.175	1.326	1.277
(4,4)	1.141	1.144	1.219	1.185	1.324	1.294
(4,1)	1.126	1.106	1.398	1.590	1.608	2.448
(8,2)	1.183	1.180	1.325	1.573	1.493	2.509
(12,3)	1.205	1.205	1.333	1.582	1.468	2.502
(16,4)	1.215	1.218	1.350	1.584	1.473	2.488

Linear elements and increment of polynomial order 2 are considered.

Table 4
Effectivity indices for cell pattern (d)–(f)

(M,N)	$E_{k,d}$	$E_{o,d}$	$E_{k,e}$	$E_{o,e}$	$E_{k,f}$	$E_{o,f}$
(1,1)	2.102	1.913	1.054	1.055	1.110	1.112
(2,2)	1.512	1.758	1.120	1.119	1.107	1.107
(3,3)	1.436	1.683	1.120	1.119	1.115	1.113
(4,4)	1.403	1.630	1.121	1.119	1.120	1.117
(4,1)	1.712	3.070	1.365	1.516	1.301	1.144
(8,2)	1.764	2.814	1.414	1.624	1.256	1.143
(12,3)	1.763	2.733	1.460	1.662	1.239	1.148
(16,4)	1.761	2.680	1.491	1.679	1.230	1.152

Linear elements and increment of polynomial order 2 are considered.

we show the effectivity indices of the two a posteriori error estimators for different linear triangulations $\mathscr{T}_h$ given by cell patterns (a)–(f). We observe the following:

- Both a posteriori error estimators can give asymptotically upper bounds of the error $|||e|||$.
- When $a/b = 1$, both a posteriori error estimators show similar performance for all cell patterns (a)–(f); when $a/b = 4$, the a posteriori error estimator with weights appears more robust than that without weights, especially for the large deformation, e.g., cell patterns (b), (d) and (e).

The first observation is due to the Theorem 1. The second one can be explained using the target function (20). If we use the factor $\frac{1}{l(\gamma)}$ as a weight function, $\mu^{\gamma}_{K,n}$ and $\tilde{\mu}_{K,n}$ will have larger difference on a longer edge, which is reasonable since the linear function along a longer edge usually yields

Table 5
Effectivity indices for cell pattern (a)–(c)

(M,N)	$E_{k,a}$	$E_{o,a}$	$E_{k,b}$	$E_{o,b}$	$E_{k,c}$	$E_{o,c}$
(1,1)	1.009	0.991	1.097	1.013	1.037	0.988
(2,2)	1.039	1.030	1.067	1.043	0.996	0.999
(3,3)	1.047	1.040	1.064	1.036	0.999	1.003
(4,4)	1.050	1.043	1.062	1.033	1.002	1.006
(4,1)	0.925	0.920	1.038	1.042	1.172	1.148
(8,2)	0.951	0.927	1.080	1.039	1.215	1.237
(12,3)	0.964	0.932	1.099	1.035	1.227	1.259
(16,4)	0.972	0.936	1.112	1.032	1.232	1.271

Spectral/*hp* elements and increment of polynomial order 2 are considered. Due to *p*-convergence, sixth-order polynomials are used for pattern (a) while eighth-order polynomials are used for pattern (b) and (c).

a larger approximation error. Thus, weights in Eq. (20) may have a large influence on the robustness of the a posteriori error estimator for the linear elements.

For spectral/*hp* elements we enrich the local finite element space $V_h^K(v)$ by polynomial order 2. In Tables 5 and 6, we show the effectivity indices for the spectral/*hp* elements. It can be seen that the two posteriori error estimators show similar performance for all different cell patterns and different deformation, which implies that for spectral/*hp* elements the flux $\mu_{K,n}^{\gamma}$ will be mainly determined by the numerical approximation $\frac{1}{2}(\tilde{\mu}_{K,n}^{\gamma} - \tilde{\mu}_{K',n}^{\gamma})$ and the equilibration parts $\frac{1}{2}(\sigma_{K,n} - \sigma_{K',n})$ or $\frac{1}{2}l_{\gamma}^{2}(\sigma_{K,n} - \sigma_{K',n})$ becomes less important compared to the linear elements. Thus, the a posteriori error estimators are not sensitive to the weights in Eq. (20) due to the fast *p*-convergence in spectral/*hp* elements.

To give an overall measurement of the performance of the two a posteriori error estimators, we show some statistics in Table 7. We compute the mean and standard deviation of the effectivity index for the deformation $a/b = 1$ and $a/b = 4$. It can be seen that for the linear elements both mean and standard deviation of E_k are smaller than those of E_o, which implies that the weights in Eq. (20) improve effectively the robustness of a posteriori error estimator. For the spectral/*hp* elements, E_k and E_o show similar mean and standard deviation.

Table 6
Effectivity indices for cell pattern (d)–(f)

(M,N)	$E_{k,d}$	$E_{o,d}$	$E_{k,e}$	$E_{o,e}$	$E_{k,f}$	$E_{o,f}$
(1,1)	0.998	1.006	1.032	1.008	1.062	1.023
(2,2)	0.988	0.991	1.020	1.017	1.061	1.035
(3,3)	0.984	0.989	1.019	1.017	1.059	1.039
(4,4)	0.982	0.988	1.019	1.018	1.059	1.041
(4,1)	1.118	1.245	1.173	1.075	1.150	1.070
(8,2)	1.157	1.245	1.190	1.083	1.157	1.084
(12,3)	1.168	1.238	1.191	1.086	1.157	1.090
(16,4)	1.176	1.231	1.190	1.087	1.155	1.093

Spectral/*hp* elements and increment of polynomial order 2 are considered. Due to *p*-convergence, sixth-order polynomials are used for pattern (e) and (f) while eighth-order polynomials are used for pattern (d).

Table 7
Overall performance of the two a posteriori error estimators for the smooth problem

	$a/b = 1$		$a/b = 4$	
	E_k	E_o	E_k	E_o
Increment 1 for $V_h^K(v)$ (Linear elements)				
Mean	1.127	1.148	1.095	1.277
Std.	0.200	0.225	0.115	0.311
Increment 2 for $V_h^K(v)$ (Linear elements)				
Mean	1.257	1.258	1.414	1.806
Std.	0.229	0.237	0.193	0.652
Increment 2 for $V_h^K(v)$ (Spectral/hp elements)				
Mean	1.031	1.017	1.124	1.100
Std.	0.032	0.020	0.090	0.112

5.2. Singular solution: the Motz problem

We now consider the Motz problem (see Fig. 5):

$$\Delta u = 0 \quad \text{in } \Omega \tag{35}$$

subject to the boundary conditions

$$u(r,\pi) = 0, \quad 0 < r < 1, \quad \partial u/\partial \boldsymbol{n} = 0, \quad 0 < r < 1, \quad \theta = 0. \tag{36}$$

On the rest of the boundary $\partial\Omega$ we use the exact solution

$$u(r,\theta) = r^{1/2}\cos\left(\frac{1}{2}\theta\right) \tag{37}$$

as the Dirichlet boundary condition. For this problem there exist a singular point at the origin.

To study this problem we focus on the cell pattern (b) in Fig. 4. We set $B_4C/B_4B_2 = 0.9$ and $V_1B_4/V_1V_4 = 0.2$. Let $V_1B_1/V_1V_2 = a$. We change the value of a to control the deformation of the elements. The domain Ω is decomposed by a cell matrix (2, 8), which yields 128 elements. It was shown in [1] that for such a singular problem a large increment of polynomial order in the local finite element space V_h^K is necessary to get good error estimates. In this work, we consider an increment up to 4.

In Fig. 6 we plot the effectivity indices E_k and E_o versus the value of a for linear and quadratic elements with different increments in the local finite element space V_h^K. It is seen

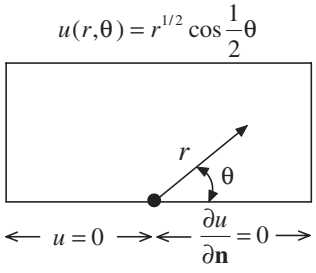

Fig. 5. Geometry and boundary conditions for the Motz problem.

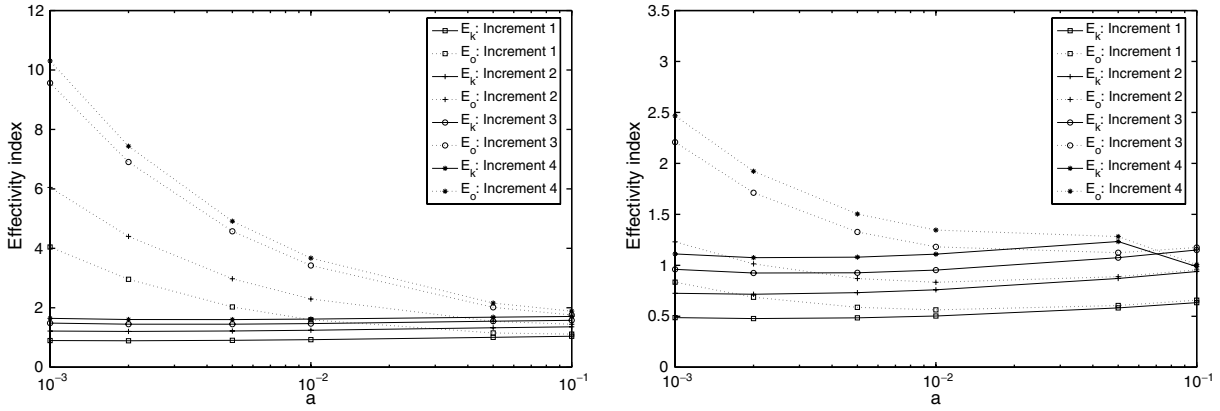

Fig. 6. Effectivity index versus the deformation of linear elements for the Motz problem. Left: $p = 1$; Right: $p = 2$.

Table 8
Effectivity indices for different meshes when $B_4C/B_4B_2 = 0.9$, $V_1B_4/V_1V_4 = 0.2$ and $V_1B_1/V_1V_2 = 0.001$

Mesh	$p = 1$		$p = 2$	
	E_k	E_o	E_k	E_o
(a)	1.453	1.729	3.217	3.213
(b)	1.216	2.381	1.112	2.467
(c)	1.283	3.135	1.081	1.327
(d)	1.278	2.495	1.514	1.641
(e)	1.251	5.331	1.137	1.620
(f)	1.307	3.193	1.081	1.326

The increments are 2 and 4 for $p = 1$ and $p = 2$, respectively, in the local finite element space V_h^K.

that for the linear elements E_o increases as a decreases while E_k remains almost the same (less than 2). For an increment of 4, $E_o > 10$ for $a = 0.001$, which means that E_o overestimates the error by an order. For this case, the weights improve the efficiency of the a posteriori error estimator significantly.

Similar behavior is observed for the quadratic elements. However, for this case E_o increases much slower as a decreases, which implies that if the numerical boundary fluxes are more accurate the error estimator will be less sensitive to the equilibration of boundary fluxes. We note that for this case an increment of 4 is necessary for E_k to give an upper bound of the true error.

We study next the dependence of the a posteriori error estimators on the meshes. We set $B_4C/B_4B_2 = 0.9$, $V_1B_4/V_1V_4 = 0.2$ and $a = 0.001$. The effectivity indices for different meshes are shown in Table 8. It is seen that the weights can, in general, improve the efficiency of the a posteriori error estimator for a large deformation, especially in linear elements.

6. Summary

In this paper we presented explicit formulas of the equilibrated fluxes used in the flux-type a posteriori error estimators and investigated a different target function for the equilibrated fluxes. We applied the obtained a posteriori error estimator to elliptic problems with smooth and singular solutions. The numerical studies show that for large element deformation and low-order polynomials the new equilibrated fluxes are, in general, more robust. For spectral/*hp* elements with high-order polynomials, it is less important how to choose the equilibrated fluxes due to the *p*-convergence. Since the cost for the equilibrated fluxes is reduced significantly, the a posteriori error estimator given in [6] can be adopted into the adaptive spectral/*hp* element method more efficiently. However, we obtain only the explicit formulas for the two-dimensional case. In the three-dimensional case, the equilibrated fluxes for edge functions can be obtained using the same formulas for the two-dimensional vertex functions. It is still not clear how to obtain explicitly the equilibrated fluxes for three-dimensional vertex functions. One possible way to simplify the procedure is to hybrid the procedures of implicit a posteriori error estimates and equilibrated fluxes, in other words, we can first impose mean fluxes on some faces to make the singular matrices for the vertex functions the same as those for two-dimensional vertex functions. Then we can get the explicit equilibrated fluxes using the formulas in this work. Since we pick up one choice of the equilibrated fluxes, we should obtain an asymptotically guaranteed error bound. However, the performance of the obtained equilibrated fluxes needs to be studied numerically.

Acknowledgements

This work was supported by the Computational Mathematical program of AFOSR. I would like to thank Professor George Em Karniadakis for useful discussions.

References

[1] M. Ainsworth, J.T. Oden, A procedure for a posteriori error estimation for *h–p* finite element methods, Comput. Methods Appl. Mech. Engrg. 101 (1992) 73–96.

[2] R. Verfürth, A Review of A Posteriori Error Estimation and Adaptive Mesh-Refinement Techniques, John Wiley & Sons Ltd. and B.G. Teubner, 1996.
[3] M. Ainsworth, J.T. Oden, A Posteriori Error Estimation in Finite Element Analysis, John Wiley & Sons, Inc., 2000.
[4] I. Babuška, T. Strouboulis, The Finite Element Method and its Reliability, Oxford University Press, 2001.
[5] I. Babuška, W. Rheinboldt, A posteriori error estimates for the finite element method, Int. J. Numer. Methods Engrg. 12 (1978) 1597–1615.
[6] M. Ainsworth, J.T. Oden, A posteriori error estimators for second order elliptic systems: Part 1. theoretical foundations and a posteriori error analysis, Comput. Math. Appl. 25 (1993) 101–113.
[7] M. Ainsworth, J.T. Oden, A posteriori error estimators for second order elliptic systems: Part 2. An optimal order process for calculating self-equilibrating fluxes, Comput. Math. Appl. 25 (1993) 75–87.
[8] R.E. Bank, A. Wieser, Some a posteriori error estimates for elliptic partial differential equations, Math. Comput. 44 (1985) 283–301.
[9] R.E. Bank, R.K. Smith, A posteriori error estimates based on hierarchical bases, SIAM J. Numer. Anal. 30 (1993) 921–935.
[10] O.C. Zienkiewicz, J.Z. Zhu, The superconvergent path recovery and a posteriori error estimates. Part i: the recovery technique, Int. J. Numer. Methods Engrg. 33 (1992) 1331–1364.
[11] O.C. Zienkiewicz, J.Z. Zhu, The superconvergent path recovery and a posteriori error estimates. Part ii: error estimates and adaptivity, Int. J. Numer. Methods Engrg. 33 (1992) 1365–1382.
[12] S. Prudhomme, J.T. Oden, On goal-oriented error estimation for elliptic problems: Application to the control of pointwise errors, Comput. Methods Appl. Mech. Engrg. 176 (1999) 313–331.
[13] J.T. Oden, S. Prudhomme, Goal-oriented error estimation and adaptivity for the finite element method, Comput. Math. Appl. 41 (2001) 735–756.
[14] P. Ladevèze, D. Leguillon, Error estimate procedure in the finite element method and applications, SIAM J. Numer. Anal. 20 (1983) 485–509.
[15] D.W. Kelly, The self-equilibration of residuals and complementary a posteriori error estimates in the finite element method, Int. J. Numer. Method Engrg. 20 (1984) 1491–1506.
[16] G.E. Karniadakis, S.J. Sherwin, Spectral/hp Element Methods for CFD, second ed., Oxford University Press, 2005.
[17] P. Ladevèze, J.P. Pelle, P. Rougeot, Error estimation and mesh optimization for classical finite elements, Engrg. Comput. 9 (1991) 69–80.
[18] C. Hirsch, Numerical Computation of Internal and External Flows, John Wiley & Sons Ltd., 1988.
[19] I. Babuška, C.S.U.T. Strouboulis, S.K. Gangaraj, K. Copps, Validation of a posteriori error estimators by numerical approach, Int. J. Numer. Methods Engrg. 37 (1994) 1073–1123.
[20] M. Ainsworth, D.W. Kelly, A posteriori error estimators and adaptivity for finite element approximation of non-homogeneous Dirichlet problem, Adv. Comput. Math. 15 (1–4) (2001) 3–23.